JOURNAL OF THERMOPHYSICS AND HEAT TRANSFER
Vol. 19, No. 4, October–December 2005

Model of Tellurium- and Zinc-Doped Indium Antimonide Solidification in Space

Alexei V. Churilov* and Aleksandar G. Ostrogorsky†
Rensselaer Polytechnic Institute, Troy, New York 12180

Numerical simulations were performed to determine the effect of residual microaccelerations on the distribution of dopants (Te and Zn) during solidification of InSb in space. A moving geometry model was developed and used to account for the reduction in melt size during growth. The model demonstrates that diffusion controlled segregation in doped InSb can be obtained at $10^{-5}g_0$ gravity for the considered growth parameters. The results for the moving geometry and semi-infinite melt domain models are compared to each other and to the analytical correlations for the case of diffusion-controlled segregation.

Nomenclature

C = solute concentration, 1/cm^3
C_{inf} = solute concentration on the opposite to the interface side of the semi-infinite domain, 1/cm^3
C_l = solute concentration in the liquid, 1/cm^3
C_s = solute concentration in the solid, 1/cm^3
C_0 = initial solute concentration, 1/cm^3
c_p = specific heat, J/kg · K
D_l = solute diffusion coefficient, m^2/s
d = ampoule inside diameter, mm
f = frequency, Hz
f_s = fraction solidified, x/L
Gr = Grashof number, $\beta g \Delta T L^3/\nu^2$
g = gravitational acceleration, m/s^2
g_0 = Earth gravitational acceleration, 9.81m/s^2
h = convective heat transfer coefficient, W/m^2 · K
J = solutal flux, 1/m^2 · s
k = thermal conductivity, W/m · K
k_0 = equilibrium segregation coefficient, C_s/C_l
L = initial melt length, cm
Pe = thermal Péclet number, RL/α
Pe_s = solutal Péclet number, $L/(D_l/R)$
Pr = Prandtl number, ν/α
q = heat flux, W/m^2
R = growth rate, cm/h
Ra = Rayleigh number, $\beta g \Delta T L^3/\alpha\nu$, $GrPr$
Re = Reynolds number, UL/ν
Sc = Schmidt number, ν/D_l
St = Stanton number, $c_p \Delta T/\Delta H_m$
T = temperature, K
t = time, s
U = velocity, m/s
V_{tan} = tangential velocity (parallel to the interface), μm/s
$\boldsymbol{v}$ = velocity vector, m/s
x, y = Cartesian coordinates, cm
α = thermal diffusivity, m^2/s
β = thermal expansion coefficient, 1/K
ΔH_m = latent heat of fusion, J/kg
ΔT = $T_h - T_m$
μ = dynamic viscosity, kg/m · s
ν = kinematic viscosity, m^2/s
ρ = density, kg/m^3
τ = dimensionless time, $R^2 t/4D_l$

Subscripts

B = bulk
h = hot
l = liquid
m = melting temperature
s = solid
seg = segregated
x = along axis x

Presented as Paper 2004-1309 at the AIAA 42nd Aerospace Sciences Meeting and Exhibit, Reno, NV, 6–10 January 2004; received 20 February 2004; revision received 27 January 2005; accepted for publication 30 January 2005.

*Graduate Student and Research Assistant, Mechanical Engineering Department. Student Member AIAA.
†Professor, Mechanical Engineering Department. Associate Fellow AIAA.

Introduction

INDIUM antimonide is of interest for the production of magnetoresistors, infrared detectors, and charge-coupled device cameras sensitive to wavelengths up to 6.5 μm. To manufacture quality devices, the semiconductor must have known constant properties, which can not be obtained without uniform dopant segregation. The most uniform dopant segregation is obtained during diffusion-controlled growth because the middle section of the ingot has a flat segregation profile. However, this is impossible to realize on Earth because of buoyancy-driven convection in the melt. The intensity of natural convection in the melt is characterized by dimensionless Rayleigh number. On Earth for the considered geometry, melt properties and temperature gradient, Rayleigh number is of the order of $\sim 10^5$, causing a complex, continuously changing convection pattern, which is very difficult to model. In space laboratories, microacceleration (g-jitter) has random direction and magnitude in the range from 10^{-4} to $10^{-6}g_0$, with the average around $10^{-5}g_0$. When crystals are grown in space, Rayleigh number is reduced to approximately 1, and the process and its analysis are greatly simplified.

Numerical Model

Numerical simulations were performed for semi-infinite melt domain and finite domain with moving geometry.

The governing equations follow.

Continuity:

$$\nabla \cdot \boldsymbol{v} = 0 \tag{1}$$

Navier–Stokes:

$$\frac{\partial \boldsymbol{v}}{\partial t} + (\boldsymbol{v} \cdot \nabla)\boldsymbol{v} = \nu \nabla^2 \boldsymbol{v} + \beta(T - T_m)\boldsymbol{g} \tag{2}$$

Energy conservation:

$$\rho_0 c_p \left(\frac{\partial T}{\partial t} + (\boldsymbol{v} \cdot \boldsymbol{\nabla}) T \right) = k \nabla^2 T \tag{3}$$

Solute conservation:

$$\frac{\partial C}{\partial t} + (\boldsymbol{v} \cdot \boldsymbol{\nabla}) C = D_l \nabla^2 C \tag{4}$$

The governing equations for heat, mass and momentum transfer were simultaneously solved using the finite element code NEKTON.[1] The following key assumptions were used to simplify the model: 1) two-dimensional mesh, 2) constant average residual microacceleration, 3) uniform initial melt concentration, 4) latent heat release due to phase change neglected, 5) constant growth rate, 6) flat stable solid–liquid interface, and 7) no solid-state diffusion.

Constant average residual microacceleration is a commonly used assumption for numerical modeling of the fluid flow in reduced gravity. It has been used by many authors in the past.[2–6] Some simulations have been done using pulsing and oscillating accelerations of low frequency or multicomponent superposition of several different frequencies and magnitudes.[7,8] In fact, they are random, and most of them are attributed to high-frequency vibrations that have little effect on convection in microgravity.[2] The assumption is valid under optimal microgravity conditions when the spacecraft does not perform any maneuvers. Crystal growth experiments are not disturbed by high-frequency oscillations ($f > 1$ Hz), caused by running machines and activities of astronauts. It was demonstrated numerically that lateral accelerations (parallel to the interface) have a significant influence on melt flow and dopant segregation.[7,9] However, the same authors provide experimental evidence that oscillating accelerations result in much smaller perturbation of the flow.[9] Accelerations as high as $10^{-3} g_0$ occur for very short times (<1 s), insufficient to establish the flow. Therefore, for the frequency range $f > 1$ Hz, a level of about $10^{-5}, \ldots, 10^{-3}$ can indeed be considered as a typical average of residual acceleration.[2] The implication of the constant average residual acceleration assumption is that it does not change its direction during the simulation, which leads to stronger radial segregation. The goal of this work is not to reproduce the exact convective pattern in the melt, but to demonstrate the effect of little gravitational disturbance as opposed to zero gravity.

Semiconductors are often doped with a minute amount of impurity that changes their electrical properties. Based on property values and growth parameters shown in Tables 1 and 2 (density, thermal expansion coefficient, temperature and concentration gradients, and low solute concentration), thermal buoyancy forces are approximately three orders of magnitude higher than solutal buoyancy forces. Therefore, the effect of the solutal buoyancy on convection was neglected (dilute system).

Energy conservation at the solid–liquid interface states that heat conduction flux in the solid is equal to the conduction flux in the liquid plus heat release at the interface per unit area,

$$q_s = q_l + \rho \Delta H_m R \tag{5}$$

Because of the low growth rate R and small Pe (Table 2), the second term in Eq. (5) can be neglected. The error associated with this assumption is estimated by the ratio of the two terms on the right-hand side:

$$\frac{\rho \Delta H_m R}{q_l} \cong \frac{\rho \Delta H_m R}{k \Delta T / L} = \frac{\Delta H_m R L}{\alpha c_p \Delta T} = \frac{\Delta H_m (RL/\alpha)}{c_p \Delta T} = \frac{Pe}{St} = 0.033 \tag{6}$$

Because the axial temperature gradient in the melt was much higher than the radial temperature gradient, the interface was observed to be nearly flat in the ground-based experiments. For simplicity, the shape of the interface was assumed to be flat in the numerical model.

The thermophysical properties of InSb used in present calculations are given in Table 1. There is a significant disagreement in the available data for the diffusion coefficients of Te and Zn in molten InSb, and so we had to choose them from the range of published values,[10–17] typical for molten semiconductor systems. Considering

Table 2 Growth parameters

Parameter	Value
Growth rate R, cm/h	0.5
Axial temperature gradient dT/dx, K/cm	60
Residual acceleration, m/s^2	$10^{-5} g_0$
Initial solute concentration C_0, cm^{-3}	5×10^{18}
Thermal Péclet number Pe	7.7×10^{-3}
Solutal Péclet number Pe_s	42
Stanton number St	0.23
Ampoule diameter d, mm	12
Initial melt length L, mm	30

Table 1 Properties of molten InSb

Property	Value	Ref.
Thermal conductivity k, W/m · K	9.23[a]	10, 11
	17.7	12
	12.3	13
	17.1	14
Density ρ, kg/m^3	6.48×10^3	11, 15
	6.47×10^3[a]	10
Specific heat c_p, J/kg · K	263[a]	10, 11
	283	15
Dynamic viscosity μ, kg/m · s	2.138×10^{-3}[a]	11
	1.941×10^{-3}	10
	2.34×10^{-3}	15
Solidification temperature T_m, K	525[a]	11
	527	10
Thermal expansion coefficient β, 1/K	1.0×10^{-4}[a]	11
	9.81×10^{-5}	15
Latent heat of fusion ΔH_m, J/kg	2.06×10^5	16
Diffusivity of Te in InSb D_l, m^2/s	1×10^{-9}	17
Diffusivity of Zn in InSb D_l, m^2/s	1×10^{-9}	17
Equilibrium segregation coefficient of Te in InSb, k_0	0.5[a]	
	0.47, . . . ,1	16
Equilibrium segregation coefficient of Zn in InSb, k_0	2.9[a]	
	2.3, . . . ,3.5	16
Prandtl number Pr	0.061	
Schmidt number Sc	330.4	

[a] Value used in calculations.

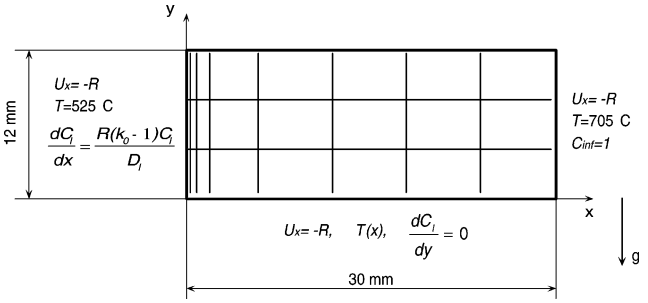

Fig. 1 Mesh and boundary conditions.

the low melt temperature, we have used $D_l = 10^{-5}$ cm^2/s for both dopants in the present study.

Semi-Infinite Melt Domain

In this section, the semi-infinite liquid domain assumption was used along with the previously listed assumptions. The computational domain for the semi-infinite melt and fixed geometry is shown in Fig. 1. The temperature was specified at all boundaries. The axial temperature gradient $\mathrm{d}T/\mathrm{d}x = 60$ K/cm. Initial temperature field was obtained by solving the steady-state heat conduction equation, uncoupled from the velocity. There are no-slip boundary conditions on side walls. The velocity was set equal to the growth rate R at all boundaries. The initial conditions in the x direction are $U_x(y) = -R$ and in the y direction are $U_y(x) = 0$. Calculations were performed for a 30-mm-long melt inside of a 12-mm-diam ampoule (12 mm i.d.) using a 12×30 mm two-dimensional mesh. Each macroelement of the mesh contains an internal 5×5 node mesh.

Solute concentration was nondimensionalized by dividing the concentration by the initial concentration in the melt ($C_0 = 1$). Opposite to the interface side of the domain was at $C_l = 1$ all of the time.

Solute transport at the solid–liquid interface was calculated from the Stefan solute mass balance (see Ref. 18), that is, balance of the flux of solute rejected from the solid–liquid interface, J_{seg}, against the solutal flux J_B, transported away from the interface. The fluxes for segregation and diffusion are, respectively,

$$J_{\mathrm{seg}} = (C_l - C_s)R \tag{7}$$

$$J_B = -D_l \frac{\mathrm{d}C_l}{\mathrm{d}x} \tag{8}$$

Local equilibrium at the solid–liquid interface defines the equilibrium distribution coefficient k_0, which can be substituted to yield

$$D_l \frac{\mathrm{d}C_l}{\mathrm{d}x} = R(k_0 - 1)C_l \tag{9}$$

Equation (9) is the convective boundary condition for concentration field, where the term $R(k_0 - 1)$ is similar to the thermal heat transfer coefficient h.

Moving Geometry

The moving geometry model, used in this section, is closer to the real experimental conditions because during the crystal growth process, the amount of melt is constantly being reduced. The reduction of melt size was achieved using NEKTON's option of a moving geometry, assigning the origin of the coordinate system to the solid–liquid interface and specifying the wall and mesh velocity equal to the growth rate $-R$ (Fig. 1). The concentration field boundary condition at the hot side of the melt (opposite to the solid–liquid interface) was set to insulated, $\mathrm{d}C_l/\mathrm{d}x = 0$ (Fig. 1). This model was used to determine if the changing melt size affects the initial segregation transient.

Results and Discussion

This numerical study was performed to simulate and analyze the Solidification Using a Baffle in Sealed Ampoules (SUBSA)[19–22] space experiments, conducted at the International Space Station in 2002, which defined the key parameters used in the model (the axial temperature gradient, the growth rate, and the geometry). These parameters are given in Table 2. The direction of gravity was set parallel to the interface (horizontal configuration), to induce the highest velocities in the melt.

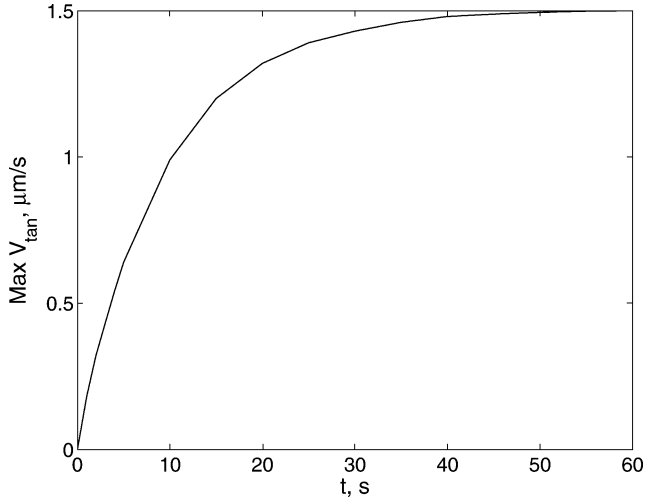

Fig. 2 Maximum tangential velocity next to interface.

To determine the time required to establish steady flow, maximum tangential velocity next to the interface was plotted as a function of time (Fig. 2). Starting with initial zero tangential velocity, it took 45 s to reach the steady flow condition.

Figure 3 shows the results of modeling with moving geometry. Figures 3a, 3c, 3e, and 3g show the velocity field; Figs. 3b, 3d, 3f, and 3h show the concentration field. The legends on velocity field (Figs. 3a, 3c, 3e, and 3g) show the scale of the flow velocity in random direction. The contour lines in the concentration field (Figs. 3b, 3d, 3f, and 3h) show the values of maximum and minimum C_l/C_0. At the beginning of solidification (after 3.5 min), for $10^{-5} g_0$, fluid velocities are of the same order of magnitude as growth rate R (Fig. 3a). Because the amount of melt is gradually decreasing, velocities decrease accordingly, and, toward the end of growth, they almost vanish. Figures 3a, 3c, 3e, and 3g show the continuous damping of velocities due to reduction of melt size. The length of Figs. 3 shrinks because of the solidification process. The melt becomes solid during the solidification, and its amount is decreased due to a finite volume of the material. The origin of coordinates is attached to the solid–liquid interface (on the left of Figs. 3a–3h). The results of solidification modeling with moving geometry have not been published in the past. It is very important to account for the fact that the melt size is reducing during crystal growth. The reduction affects the convection in the melt, which changes the dopant distribution in the solid crystal.

Throughout the growth process, the dopant atoms rejected at the interface are exposed to melt convection. This produces an asymmetric shape of the solute boundary layer, causing radial segregation. However, Figs. 3b, 3d, 3f, and 3h show that flow velocity has no effect on the composition of the bulk melt.

The results of modeling with fixed geometry and semi-infinite melt domain have been compared to the Tiller et al.[23] equation:

$$C_s = C_0\big((1 - k_0)\{1 - \exp[-k_0(R/D)x]\} + k_0\big) \tag{10}$$

and Memelink's[24] equation:

$$C_s = \tfrac{1}{2}C_0\Big[1 + \operatorname{erf}\Big[\sqrt{\tau}\Big] - (1 - 2k_0)\exp[-4k_0(1 - k_0)\tau] \times \Big\{1 + \operatorname{erf}\Big[(1 - 2k_0)\sqrt{\tau}\Big]\Big\}\Big] \tag{11}$$

where $x = Rt$ is the position in the solid. Note that Eq. (11) is identical with that of Smith et al.,[25] but derived using a different mathematical procedure.

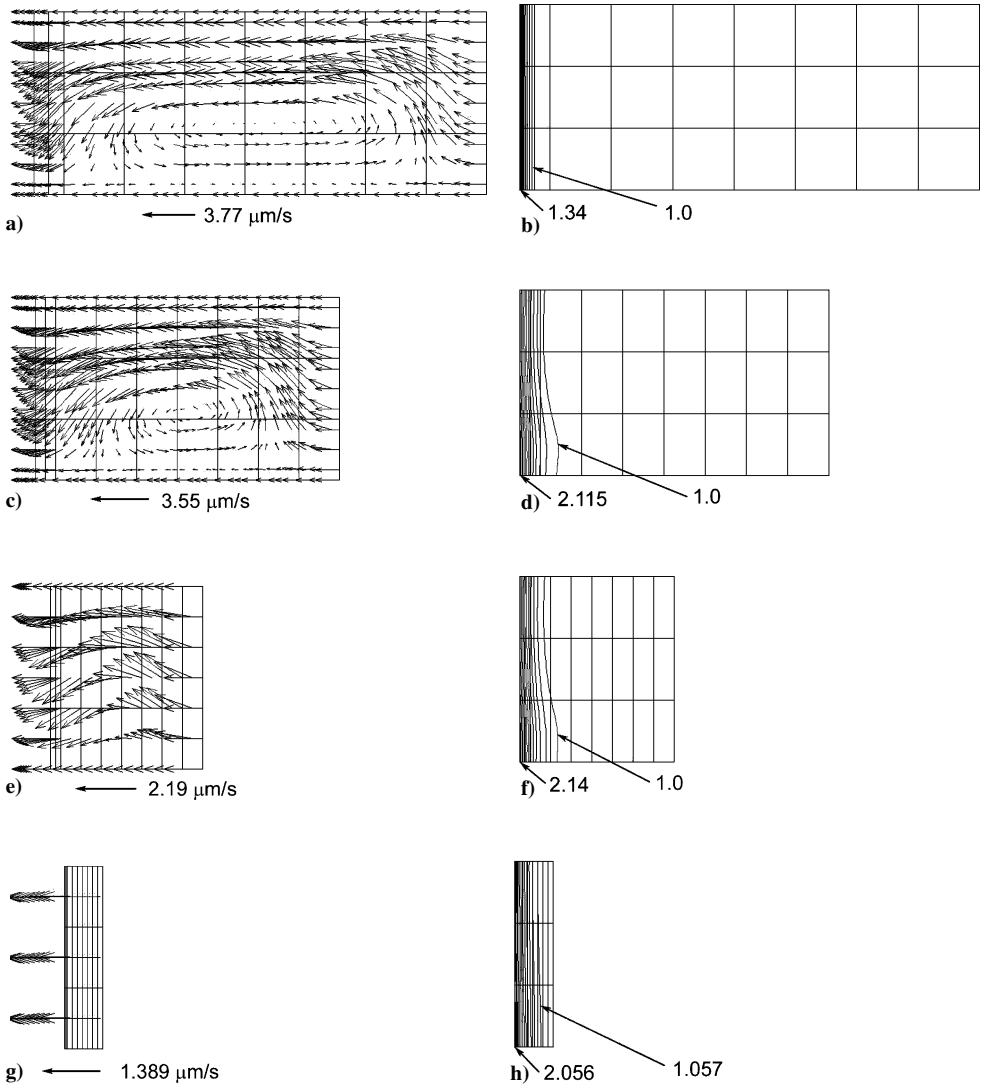

Fig. 3 Numerical modeling of InSb:Te growth with moving geometry; maximum C_l/C_0 is maximum solute concentration at interface; minimum C_l/C_0 is minimum solute concentration away from interface: a) t = 3.5 min, maximum tangential velocity 2.6 mm from interface V_{tan} = 1.5 μm/s; b) t = 3.5 min, maximum C_l/C_0 = 1.34; c) t = 2 h, maximum V_{tan} = 1.5 μm/s at 2.6 mm from interface; d) t = 2 h, maximum C_l/C_0 = 2.115; e) t = 4 h, maximum V_{tan} = 0.95 μm/s at 2 mm from interface; f) t = 4 h, maximum C_l/C_0 = 2.139; g) t = 5.5 h, maximum V_{tan} = 0.022 μm/s at 0.5 mm from interface; and h) t = 5.5 h, maximum C_l/C_0 = 2.056, minimum C_l/C_0 = 1.057.

Using the moving geometry, we can observe the final segregation transient. The segregation profiles obtained using the moving geometry model were compared to the analytical results of the Smith et al.[25] equation for the final transient:

$$\frac{C_s(\hat{x})}{C_0} = 1 + \sum_{n=1}^{\infty}(2n+1)\frac{\prod(n-k_0)}{\prod(n+k_0)} \times \exp[-n(n+1)Pe_s(1-f_s)] \tag{12}$$

where

$$Pe_s \equiv \frac{L}{D_l/R} \approx \frac{\text{system length}}{\text{characteristic diffusion length}} \tag{13}$$

is the solutal Péclet number. For the given system, $L = 3$ cm and $Pe_s = 42$.

Figure 4 shows the segregation profiles obtained using the fixed geometry (semi-infinite melt domain) model. The descending and ascending curves show the distribution of Zn and Te, respectively. The lengths of the initial transients differ because given dopants have different segregation coefficients. Because the flow at $10^{-5}g_0$

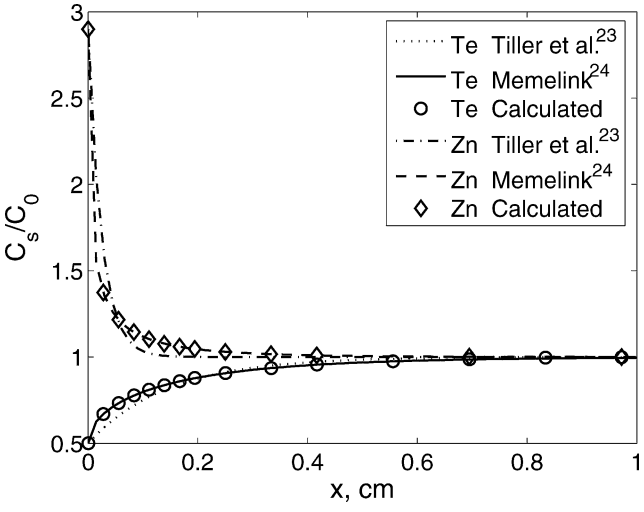

Fig. 4 Te and Zn distribution in solid InSb, R = 5 mm/h, dT/dx = 60 K.

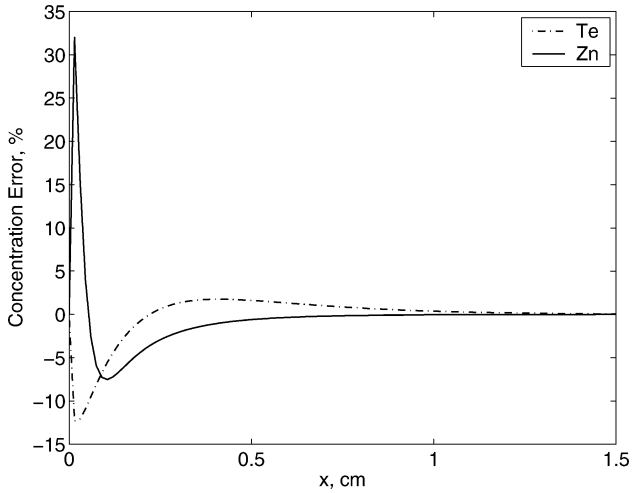

Fig. 5 Difference between concentrations in the solid calculated using the Tiller et al. [Eq. (10)] and Memelink [Eq. (11)] equations as a function of distance.

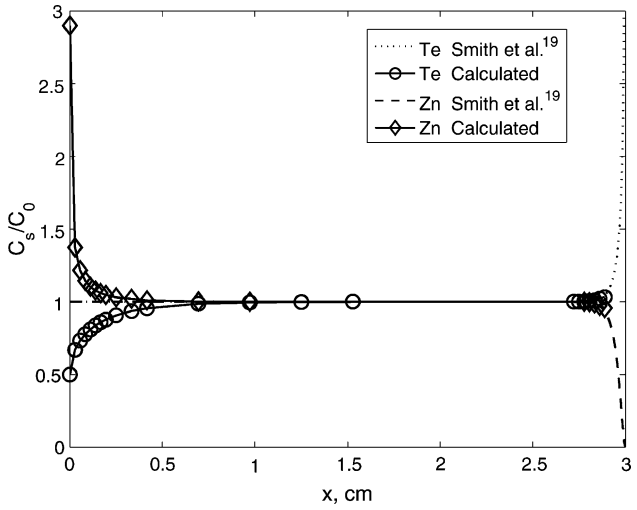

Fig. 6 Segregation of Te and Zn calculated using moving geometry; R = 5 mm/h, dT/dx = 60 K.

does not cause significant dopant transport in the melt, the segregation curves for zero gravity and $10^{-5}g_0$ overlap; the values of C_s calculated at $g = 0$ and at $10^{-5}g_0$ agree within four digits of accuracy. (Maximum error is less than 0.1%.) The simulation results are shown as one curve for both gravity values.

The initial transient length, calculated using the Tiller et al. approximation [here Eq. (10)], notably differs from the other curves (up to 30% for Te and 78% for Zn). The end of the transient was defined as the point at which the concentration is within 1% from C_0. Figure 5 shows the error, calculated as the difference between the results of the Tiller et al. approximation and Memelink's exact solution, divided by the latter. When the error is equal to zero, the curves intersect at that point. Memelink's equation [here Eq. (11)] is in full agreement with the numerical modeling results (maximum error <0.1%).

Figure 6 shows the results of simulation with the moving geometry model. The curves display the initial segregation transient and the beginning of the final transient. The final transient is much shorter, as can be seen from Fig. 6. Simulations were done for zero gravity and $10^{-5}g_0$, and the results are within 0.1% maximum error. One curve in Fig. 6 represents the results of both simulations. The simulation terminated at the point when the melt was only 1 mm long because after this point the mesh was too distorted to allow further calculation. The magnified section of the final transient, in Fig. 7, shows the numerically obtained results and those calculated using the Smith et al.[25] analytical solution, which are in excellent agreement (maximum error <0.1%).

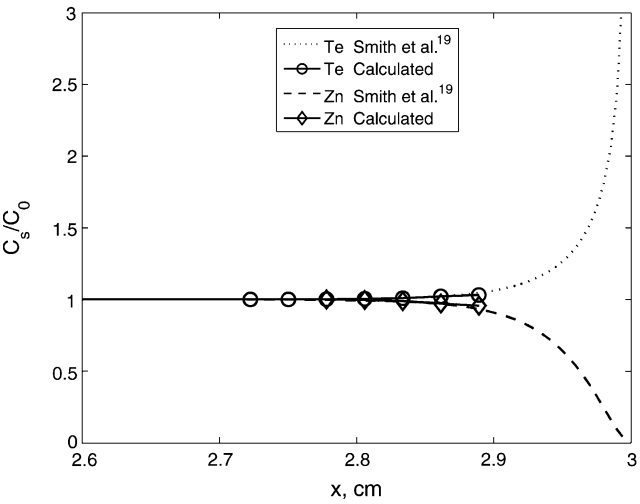

Fig. 7 Final transient of segregation.

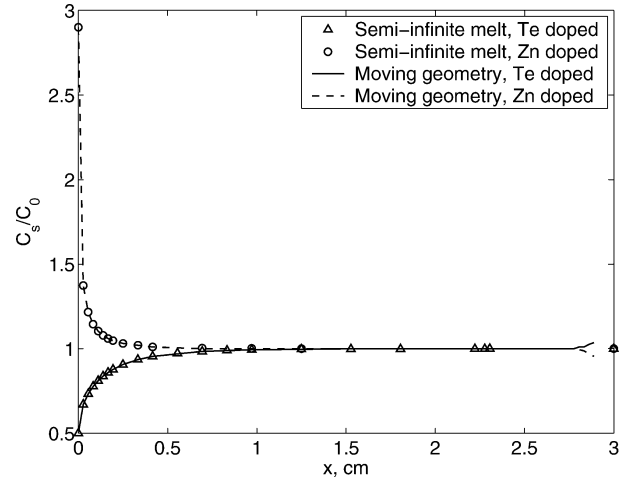

Fig. 8 Segregation calculated using fixed geometry model vs calculated with moving geometry; $10^{-5}g_0$, R = 5 mm/h, dT/dx = 60 K.

The results obtained using the moving and fixed geometry models are compared in Fig. 8. There is no visible difference between the results of the two models (maximum error <0.1%). The curves overlap in the first 28 mm. Therefore, the fixed geometry model can be successfully used if the Péclet number is relatively high, that is, system length is much greater than diffusion length.

The accuracy of NEKTON to simulate buoyancy-driven flow was tested by Vogel,[3] by plotting the Reynolds number vs Grashof number, calculated using NEKTON. The expected relation was produced: Reynolds number is proportional to Grashof number at low values, but becomes proportional to the square root of Grashof number at high values. The agreement itself between NEKTON results and analytical correlations [Eqs. (11) and (12)] is a validation for the code's accuracy in simulating axial solute segregation, for the conditions and assumptions of this paper.

Conclusions

The present numerical calculations demonstrate that $10^{-5}g_0$ acceleration has negligible effect on segregation of Te and Zn in InSb for growth parameters used in SUBSA investigation. Therefore, diffusion-controlled segregation can be obtained during SUBSA crystal growth experiments in space, provided that the assumptions made are valid. Numerical simulations performed for this study confirm the results of previous calculations with semi-infinite melt domain models.[3,4] The results of dopant segregation modeling with moving geometry have been reported for the first time.

It has been established that the simple Tiller et al. equation [here Eq. (10)] tends to underestimate the length of the initial segregation transient. The Smith et al. equation [here Eq. (12)] and Memelink's equation [here Eq. (11)] are exact solutions, and they predict the segregation in zero gravity very precisely. The agreement of these analytical solutions with our numerical simulations is excellent. The curves of numerical and analytical results are almost identical (maximum error $<0.1\%$).

Acknowledgment

This work is sponsored by the Microgravity Science and Applications Division of NASA (Contract NCC8-97).

References

[1]NEKTON 2.85 User's Manual, 1994.

[2]Seifert, W., and Reinshaus P., "Axial Solute Transport During Bridgman Growth of BiSbTe3-Mixed Crystals—A Comparison of Analytical and Numerical Results," *Crystal Research and Technology*, Vol. 35, No. 1, 2000, pp. 5–18.

[3]Vogel, M., and Ostrogorsky, A. G., "Directional Solidification Using Baffle in Microgravity," *Acta Astronautica,* Vol. 48, No. 2-3, 2001, pp. 93–100.

[4]Marin, C., and Ostrogorsky, A., "Control of Convection During Directional Solidification in Terrestrial and Low Gravity," *Proceedings of the SPIE*, Materials Research in Low Gravity II, Vol. 3792, The International Society for Optical Engineering, Bellingham, WA, 1999, pp. 112–123.

[5]Buhrig, E., Schwichtenberg, G., and Patzold, O., "Growth of Zn-doped Germanium Under Microgravity," *Crystal Research and Technology*, Vol. 35, No. 8, 2000, pp. 911–919.

[6]Kassemi, M., Kaforey, M., and Matthiesen, D., "Effect of Void-Generated Thermocapillary Convection on Dopant Segregation in Microgravity Solidification," *Journal of Thermophysics and Heat Transfer*, Vol. 15, No. 2, 2001, pp. 219–227.

[7]Alexander, J. I. D., Ouazzani, J., and Rosenberger F., "Analysis of the Low Gravity Tolerance of Bridgman–Stockbarger Crystal Growth. I. Steady and Impulse Accelerations," *Journal of Crystal Growth*, Vol. 97, No. 2, 1989, pp. 285–302.

[8]Alexander, J. I. D., Amiroudine, S., Ouazzani, J., and Rosenberger, F., "Analysis of the Low Gravity Tolerance of Bridgman–Stockbarger Crystal Growth. II. Transient and Periodic Accelerations," *Journal of Crystal Growth*, Vol. 113, No. 1-2, 1991, pp. 21–38.

[9]Alexander, J. I. D., Garandet, J.-P., Favier, J.-J., and Lizée, A., "g-Jitter Effects on Segregation During Directional Solidification of Tin-Bismuth in the MEPHISTO Furnace Facility," *Journal of Crystal Growth*, Vol. 178, No. 4, 1997, pp. 657–661.

[10]Glasov, V. M., Chizhevskaya, S. N., and Glagoleva, N. N., Liquid Semiconductors, Plenum Press, New York, 1969.

[11]Müller, G., and Ostrogorsky, A., *Handbook of Crystal Growth*, Vol. 2, North-Holland/Elsevier, Amsterdam, 1994, p. 812.

[12]Nakamura, S., Hibiya, T., and Yamamoto, F., "Thermal Conductivity of GaSb and InSb in Solid and Liquid States," *Journal of Applied Physics*, Vol. 68, No. 10, 1990, pp. 5125–5127.

[13]Amirkhanov, K., and Magomedov, Y. B., "InSb Thermal Conductivity in Solid and Liquid States," *Soviet Physics of Solid State*, Vol. 7, No. 2, 1965, pp. 637–640.

[14]Fedorov, V. I., and Machuev, V. I., "Thermal Conductivity of Gallium, Indium, and Thallium Antimonides," *Teplofizika Vysokikh Temperatur*, Vol. 8, No. 2, 1970, pp. 447–449.

[15]Nakamura, S., and Hibiya, T., "Thermophysical Properties of Molten Semiconductors," *International Journal of Thermophysics*, Vol. 13, No. 6, 1992, pp. 1061–1084.

[16]Hellwege, K.-H., and Madulung, O. (eds.), *Landolt–Börnstein*, Group III, Vol. 17, Subvol. d, Springer-Verlag, Berlin, 1984, pp. 16–22.

[17]Ostrogorsky, A. G., Sell, H. J., Scharl, S., and Müller, G., "Convection and Segregation During Growth of Ge and InSb Crystals by the Submerged Heater Method," *Journal of Crystal Growth*, Vol. 128, No. 1-4, 1993, pp. 201–206.

[18]Bejan, A., *Heat Transfer*, Wiley, New York, 1993, p. 187.

[19]Flinn, E., "Glovebox Fits Astronauts to a 'T'," *Aerospace America*, Aug. 2002, pp. 18–19.

[20]"Scientists to Study Bubbles and Semiconductors in Space," *Chemical Engineering Progress*, Vol. 98, No. 8, 2002, pp. 18–20.

[21]"Space for Materials Research," *Materials Today*, Sept. 2002, p. 17.

[22]Ostrogorsky, A. G., Marin C., Churilov, A., Volz, M., Bonner, W. A., Spivey, R. A., and Smith, G., "Solidification Using the Baffle in Sealed Ampoules," AIAA Paper 2003-1309, Jan. 2003.

[23]Tiller, W. A., Jackson, K. A., Rutter, J. W., and Chalmers, B., "The Redistribution of Solute Atoms During the Solidification of Metals," *Acta Metallurgica*, Vol. 1, July 1953, pp. 428–437.

[24]Memelink, O. W., "The Distribution of Impurity in a Semi-infinite Solidified Melt," *Philips Research Reports*, Vol. 11, 1956, pp. 183–189.

[25]Smith, V. G., Tiller, W. A., and Rutter, J. W., "A Mathematical Analysis of Solute Redistribution During Solidification," *Canadian Journal of Physics*, Vol. 33, 1955, pp. 723–745.

[26]Matlab Version 6.5.0.180913a Release 13, MathWorks Inc., Natick, MA, USA, June 18, 2002.

[27]Maple Version 8.00, Waterloo Maple Inc., Waterloo, ON, Canada, April 22, 2002.